

Supporting Information

Milling-Induced ‘Turn-off’ Luminescence in Copper Nanoclusters

Subrata Duary,^a Arijit Jana,^a Amitabha Das,^b Swetashree Acharya,^a Amoghavarsha Ramachandra Kini,^a Jayoti Roy,^a Ajay Kumar Poonia,^c Deepak Kumar Patel,^a Vivek Yadav,^a P. K. Sudhadevi Antharjanam,^d Biswarup Pathak,^{*b} Adarsh Kumaran Nair Valsala Devi,^{*c} and Thalappil Pradeep^{*a}

^a DST Unit of Nanoscience (DST UNS) and Thematic Unit of Excellence (TUE), Department of Chemistry, Indian Institute of Technology, Madras, Chennai – 600036, India.

*Email: pradeep@iitm.ac.in

^b Department of Chemistry, Indian Institute of Technology Indore, Indore 453552, India.

*Email: biswarup@iiti.ac.in

^c Department of Physics, Indian Institute of Science Education and Research Bhopal, Bhopal 462066, India.

*E-mail: adarsh@iiserb.ac.in

^d Sophisticated Analytical Instrument Facility, Indian Institute of Technology Madras, Chennai 600036, India.

Table of contents

Items	Descriptions	Page No.
1	Computational details	S3
Table S1	Crystal data and structure refinement of Cu ₄ (MNA) ₂ (DPPE) ₂	S4
Table S2	Atomic coordinates and equivalent isotropic displacement parameters for Cu ₄ NC	S5-S7
Table S3	Crystal data and structure refinement of Cu ₆ (MNA-H) ₆	S8-S9
Table S4	Atomic coordinates and equivalent isotropic displacement parameters for Cu ₆ NC	S9-S11
Table S5	List of mechanoresponsive copper clusters	S11

Table S6	List of solvents for recovery of luminescence	S12
Figure S1	Synthesis and characterization of the cluster $[Cu_{18}H_{16}(DPPE)_6]^{2+}$ through UV-Vis absorption spectroscopic and mass spectrometric studies	S13
Figure S2	Stability check through UV-Vis absorption spectrum of Cu_4 and Cu_6 NCs in acetonitrile	S13
Figure S3	FESEM images and EDS elemental spectrum of Cu_4 and Cu_6 NCs	S14
Figure S4	Structures and molecular packing of Cu_4 and Cu_6 NCs along the b-axis	S 15
Figure S5	Non-covalent interactions involving crystal structures in the lattice	S16
Figure S6	ORTEP structure of Cu_4 and Cu_6 NCs	S17
Figure S7	ESI MS spectrum of sodium and potassium ions embedded to Cu_4 NC and tabulated MSMS fragments of Cu_4 and Cu_6 nanoclusters	S17
Figure S8	FTIR spectrum of Cu_4 NC	S18
Figure S9	FTIR spectrum of Cu_6 NC	S19
Figure S10	XPS spectrum of Cu_4 NC	S20
Figure S11	XPS spectrum of Cu_6 NC	S21
Figure S12	DFT optimized structural details of Cu_4 NC	S22
Figure S13	FMO and KS diagram of Cu_4	S22
Figure S14	DFT optimized structural details of Cu_6 NC	S23
Figure S15	FMO and KS diagram of Cu_6	S23
Figure S16	Photoluminescence (PL) spectrum of Cu_4 NC in solution and solid states	S24
Figure S17	PL spectrum of Cu_6 NC in solution and solid states	S24
Figure S18	PL upon oxygen exposure to solid Cu_4 NC	S25
Figure S19	PL upon oxygen exposure to solid Cu_6 NC	S25
Figure S20	Heating effect on the PL intensity of solid Cu_4 NC	S26
Figure S21	Heating effect on the PL intensity of solid Cu_6 NC	S26
Figure S22	Thermogravimetry (TG) and derivative thermogravimetry (DTG) plots of Cu_4 NC	S27

Figure S23	TG and DTG data of Cu ₆ NC	S27
2	References	

1. Computational details

Text S1:

For molecular-level DFT calculations, the Gaussian 09 D.01 program was used.⁵ The Becke's three-parameter hybrid exchange functional and Lee–Yang–Parr's (B3LYP), correlation functional with Pople's 6–31G* basis set was used for non-metal elements along with LANL2DZ-ECP (effective core potential) for Cu atoms, respectively.^{6–13}

In the TD-DFT calculations the PBEPBE and B3LYP functionals found to be accurately replicate the experimentally observed absorption bands for Cu₄ and Cu₆, respectively. All the calculations were performed implicit conductor-like polarizable continuum model (CPCM) with acetonitrile solvent ($\square = 35.09$) in order to mimic experimental conditions (J. Comput. Chem., 2003, 24, 669–681; J. Phys. Chem. A, 1998, 102, 1995–2001). To identify the orbital contribution to molecular orbitals and corresponding energies, multi wave function 3.6 was employed to perform Kohn-Sham orbital analysis.¹⁴

Vienna Ab-Initio Simulation Package (VASP) was employed for periodic boundary condition-based calculations with Generalized gradient approximation of Perdew–Burke–Ernzerhof (PBE) functional.^{15–17} The Projector augmented wave (PAW) method was used to treat ion-electron interactions.^{18–19} The ionic relaxations were carried out using a Conjugate gradient algorithm with convergence criterion of 10⁻⁴ eV for minimum energy and 0.02 eV Å⁻¹ for Hellmann-Feynman forces on atoms. Due to the large size of the unit cells of the compounds, the Brillouin zone was sampled at the Gamma point (1×1×1). For the PDOS calculation, a higher (3×3×3) K-point was used.

Table S1. Crystal data and structure refinement for Cu₄ NC

Identification code	Cu ₄ SD
Empirical formula	C ₆₄ H ₅₄ Cu ₄ N ₂ O ₄ P ₄ S ₂
Formula weight	1357.25
Temperature	173(2) K
Wavelength	0.71073 Å
Crystal system	Orthorhombic
Space group	P n a 2 ₁
Unit cell dimensions	a = 19.2367(15) Å α= 90° b = 21.2522(17) Å β= 90°. c = 14.6063(11) Å γ= 90°.
Volume	5971.4(8) Å ³
Z	4
Density (calculated)	1.510 Mg/m ³
Absorption coefficient	1.632 mm ⁻¹
F(000)	2768
Crystal size	0.238 x 0.152 x 0.038 mm ³
Theta range for data collection	3.064 to 28.301°
Index ranges	-25<=h<=25, -28<=k<=28, -19<=l<=19
Reflections collected	283464
Independent reflections	14836 [R(int) = 0.0908]
Completeness to theta = 25.242°	99.7 %
Absorption correction	Semi-empirical from equivalents
Max. and min. transmission	0.7459 and 0.6417
Refinement method	Full-matrix least-squares on F ²
Data / restraints / parameters	14836 / 1 / 722
Goodness-of-fit on F ²	1.077
Final R indices [I>2sigma(I)]	R1 = 0.0345, wR2 = 0.0726
R indices (all data)	R1 = 0.0470, wR2 = 0.0783
Absolute structure parameter	0.033(10)
Extinction coefficient	n/a
Largest diff. peak and hole	0.770 and -0.391 e.Å ⁻³

Table S2. Atomic coordinates ($\times 10^4$) and equivalent isotropic displacement parameters ($\text{\AA}^2 \times 10^3$) for Cu₄-r1. U(eq) was defined as one third of the trace of the orthogonalized U^{ij} tensor.

	x	y	z	U(eq)
Cu(1)	1882(1)	4694(1)	5328(1)	37(1)
Cu(2)	769(1)	5292(1)	4426(1)	42(1)
Cu(3)	3254(1)	4846(1)	4217(1)	37(1)
Cu(4)	4279(1)	5312(1)	5351(1)	43(1)
C(1)	1053(3)	6251(2)	3059(3)	42(1)
C(2)	1820(2)	6213(2)	3285(3)	38(1)
C(3)	2218(3)	6745(2)	3153(4)	57(1)
C(4)	2919(3)	6749(2)	3355(5)	64(2)
C(5)	3217(3)	6206(2)	3680(4)	51(1)
C(6)	2165(2)	5673(2)	3621(3)	32(1)
C(7)	3866(2)	6260(2)	6683(3)	39(1)
C(8)	3098(2)	6106(2)	6540(3)	35(1)
C(9)	2821(2)	5562(2)	6149(3)	31(1)
C(10)	1700(2)	5952(2)	6291(4)	48(1)
C(11)	1927(3)	6490(2)	6698(4)	57(1)
C(12)	2632(3)	6564(2)	6818(4)	50(1)
C(13)	-793(2)	4784(2)	4921(3)	42(1)
C(14)	-943(3)	4985(3)	4043(4)	63(2)
C(15)	-1500(4)	4757(4)	3568(5)	86(2)
C(16)	-1915(3)	4300(3)	3969(5)	82(2)
C(17)	-1767(3)	4085(3)	4818(5)	74(2)
C(18)	-1210(2)	4327(2)	5310(4)	57(1)
C(19)	-264(2)	5799(2)	6116(3)	42(1)
C(20)	-515(4)	5770(3)	6995(5)	83(2)
C(21)	-629(5)	6315(4)	7504(6)	105(3)
C(22)	-524(4)	6890(3)	7114(6)	85(2)

C(23)	-290(3)	6929(3)	6229(5)	71(2)
C(24)	-152(3)	6381(2)	5736(4)	54(1)
C(25)	204(2)	4530(2)	6347(3)	38(1)
C(26)	460(2)	3909(2)	5926(3)	36(1)
C(27)	1625(2)	3685(2)	7132(3)	39(1)
C(28)	1122(3)	3547(3)	7793(3)	60(1)
C(29)	1331(5)	3431(3)	8684(4)	89(2)
C(30)	2021(6)	3439(4)	8909(5)	102(3)

C(31)	2514(4)	3560(3)	8269(5)	86(2)
C(32)	2315(3)	3692(3)	7376(4)	57(1)
C(33)	1530(2)	3084(2)	5387(3)	35(1)
C(34)	1707(3)	3077(3)	4479(3)	57(1)
C(35)	1736(4)	2513(3)	4003(4)	80(2)
C(36)	1614(3)	1961(3)	4437(5)	76(2)
C(37)	1466(4)	1963(2)	5337(6)	87(2)
C(38)	1422(4)	2523(2)	5823(4)	70(2)
C(39)	3495(2)	3716(2)	2486(3)	39(1)
C(40)	3902(3)	3422(3)	1822(4)	61(1)
C(41)	3586(4)	3091(3)	1119(4)	77(2)
C(42)	2882(4)	3038(3)	1071(4)	75(2)
C(43)	2479(4)	3340(3)	1691(5)	73(2)
C(44)	2783(3)	3676(3)	2399(4)	54(1)
C(45)	4026(2)	3425(2)	4211(3)	38(1)
C(46)	3553(3)	3284(2)	4897(4)	49(1)
C(47)	3621(3)	2762(2)	5436(4)	61(1)
C(48)	4176(3)	2359(3)	5292(5)	70(2)
C(49)	4661(3)	2499(3)	4614(5)	74(2)
C(50)	4584(3)	3023(2)	4062(4)	60(1)
C(51)	4717(2)	4360(2)	3064(3)	46(1)
C(52)	5271(2)	4488(2)	3768(3)	47(1)
C(53)	5964(2)	5093(2)	5195(3)	44(1)
C(54)	5901(4)	4750(3)	5992(4)	64(2)
C(55)	6469(5)	4642(4)	6541(5)	86(2)
C(56)	7105(4)	4897(4)	6305(6)	88(2)
C(57)	7166(3)	5236(3)	5547(6)	83(2)
C(58)	6597(3)	5338(3)	4965(5)	66(2)
C(59)	5336(2)	5858(2)	3747(3)	43(1)
C(60)	5558(3)	5817(3)	2846(4)	60(1)
C(61)	5629(4)	6349(3)	2327(5)	78(2)
C(62)	5485(4)	6935(3)	2682(5)	81(2)
C(63)	5277(4)	6982(3)	3572(5)	76(2)
C(64)	5198(3)	6451(2)	4110(4)	58(1)

N(1)	2854(2)	5673(2)	3795(2)	35(1)
N(2)	2132(2)	5487(2)	6024(2)	36(1)
S(1)	1763(1)	4935(1)	3804(1)	34(1)
S(2)	3294(1)	4882(1)	5815(1)	34(1)
O(1)	893(2)	6515(2)	2348(3)	60(1)
O(2)	621(2)	6035(2)	3631(3)	70(1)
O(3)	4298(2)	6089(2)	6089(3)	66(1)
O(4)	4015(2)	6570(2)	7362(3)	58(1)
P(1)	-16(1)	5101(1)	5466(1)	35(1)
P(2)	1410(1)	3844(1)	5939(1)	30(1)
P(3)	3856(1)	4106(1)	3492(1)	35(1)
P(4)	5187(1)	5184(1)	4489(1)	39(1)

Table S3. Crystal data and structure refinement for Cu₆NC

Identification code	Cu ₆ SD		
Empirical formula	C ₅₇ H ₇₃ Cu ₆ N ₁₃ O ₁₉ S ₆		
Formula weight	1817.88		
Temperature	296(2) K		
Wavelength	0.71073 Å		
Crystal system	Triclinic		
Space group	P -1		
Unit cell dimensions	a = 13.248(3) Å	α= 114.754(9)°.	
	b = 13.622(3) Å	β= 96.758(10)°.	
	c = 13.881(3) Å	γ= 115.050(8)°.	
Volume	1923.8(8) Å ³		
Z	1		
Density (calculated)	1.569 Mg/m ³		
Absorption coefficient	1.863 mm ⁻¹		
F(000)	928		
Crystal size	0.267 x 0.207 x 0.070 mm ³		
Theta range for data collection	3.300 to 26.000°		
Index ranges	-16<=h<=16, -16<=k<=16, -17<=l<=17		

Reflections collected	85081
Independent reflections	7547 [R(int) = 0.1101]
Completeness to theta = 25.242°	99.8 %
Absorption correction	Semi-empirical from equivalents
Max. and min. transmission	0.7457 and 0.6283
Refinement method	Full-matrix least-squares on F ²
Data / restraints / parameters	7547 / 67 / 478
Goodness-of-fit on F ²	1.064
Final R indices [I>2sigma(I)]	R1 = 0.0454, wR2 = 0.0981
R indices (all data)	R1 = 0.0822, wR2 = 0.1196
Extinction coefficient	n/a
Largest diff. peak and hole	1.082 and -0.502 e.Å ⁻³

Table S4. Atomic coordinates (x 10⁴) and equivalent isotropic displacement parameters (Å²x 10³) for Cu₆. U(eq) is defined as one third of the trace of the orthogonalized U^{ij} tensor.

	x	y	z	U(eq)
Cu(1)	5900(1)	4151(1)	4150(1)	42(1)
Cu(2)	4372(1)	3368(1)	5155(1)	44(1)
Cu(3)	3428(1)	4015(1)	3613(1)	41(1)
C(1)	3290(4)	1424(4)	2739(4)	34(1)
C(2)	2546(4)	217(4)	1752(4)	41(1)
C(3)	1784(5)	-774(5)	1862(5)	57(1)
C(4)	1795(5)	-584(5)	2920(6)	66(2)
C(5)	2580(5)	610(5)	3857(5)	51(1)
C(6)	2499(5)	-75(4)	571(4)	51(1)
C(7)	1842(3)	2956(4)	4678(3)	32(1)
C(8)	835(4)	2082(4)	4731(4)	37(1)
C(9)	-209(4)	1288(5)	3798(5)	55(1)
C(10)	-234(5)	1368(6)	2829(5)	65(2)

C(11)	797(4)	2221(5)	2830(4)	53(1)
C(12)	872(4)	2028(5)	5793(4)	46(1)
C(13)	7017(4)	3741(4)	5780(4)	36(1)
C(14)	7760(4)	3448(4)	6256(4)	44(1)
C(15)	8557(6)	3262(6)	5757(5)	68(2)
C(16)	8570(6)	3306(7)	4780(6)	81(2)
C(17)	7774(5)	3532(6)	4332(5)	65(2)
C(18)	7697(5)	3293(5)	7253(5)	54(1)
C(19)	2394(6)	6822(6)	86(6)	72(2)
C(20)	1375(8)	6073(11)	-1859(7)	158(5)
C(21)	3562(7)	7392(8)	-1013(8)	108(3)
C(22)	1521(6)	2522(6)	8642(5)	73(2)
C(23)	1300(8)	3585(8)	10437(6)	113(3)
C(24)	1826(12)	1974(11)	10040(8)	173(6)
C(25)	6294(10)	9816(11)	2086(8)	176(6)
C(26)	6224(8)	9261(10)	3443(10)	145(4)
C(27)	5191(8)	10291(8)	3246(10)	145(4)
N(1)	3324(3)	1594(3)	3774(3)	40(1)
N(2)	7014(3)	3749(4)	4809(3)	46(1)
N(3)	1820(3)	2998(4)	3723(3)	40(1)
N(4)	2432(5)	6752(5)	-878(4)	73(1)
N(5)	1575(5)	2717(5)	9666(4)	74(2)
N(6)	5896(5)	9810(5)	2902(4)	71(1)
O(1)	3534(4)	385(4)	487(3)	79(1)
O(2)	1571(4)	-740(5)	-213(4)	98(2)
O(3)	1474(4)	1560(4)	5999(3)	63(1)
O(4)	363(5)	2384(6)	6384(4)	97(2)
O(5)	6762(4)	2740(5)	7359(5)	99(2)
O(6)	8709(3)	3775(4)	7977(3)	72(1)
O(7)	1421(5)	6347(6)	227(5)	109(2)
O(8)	1761(5)	1776(5)	7959(4)	86(1)
O(9)	6382(6)	10060(7)	1502(5)	133(3)
S(1)	4149(1)	2804(1)	2699(1)	36(1)
S(2)	3181(1)	4039(1)	5873(1)	37(1)

S(3)	6123(1)	4227(1)	6450(1)	37(1)
N(7)	5070(40)	5080(40)	0(30)	150(6)
C(28)	5150(30)	5050(40)	1020(20)	213(14)
C(29)	5010(30)	4110(30)	-870(20)	179(9)
C(30)	4270(30)	5460(40)	-220(40)	276(16)
O(10)	5060(20)	3380(20)	-600(20)	255(11)

Table S5. List of mechanoresponsive copper nanoclusters

Molecular formula	$\lambda_{\text{max.}}$ (emission)	Reference
[Cu ₄ I ₄ (PPh ₂ (CH ₂ CH=CH ₂)) ₄]	440 nm/530nm/580 nm	1
Cu ₄ I ₄ (PPh ₃) ₄	520 nm/560 nm	2
Cu ₄ (oCBT) ₄ /Cu ₄ (mCBT) ₄ /Cu ₄ (ICBT) ₄ (CBT=carborane thiol)	525nm/533nm/595nm	3
Au ₄ Cu ₂ (decz) ₂ (POP) ₂ (H ₃ decz= 3,6-di-tert-butyl-1,8- diethynyl-9H-carbazole, POP= bis(2- diphenylphosphinophenyl)ether	576 nm	4
[Cu ₄ (MNA) ₂ (DPPE) ₂] ⁺ and [Cu ₆ (MNA-H) ₆] ⁺	560 nm and 755 nm	This work

Table S6. List of solvents used for the recovery of luminescence.

Solvent	Luminescence recovery	
	Cu ₄	Cu ₆
CH ₃ OH	✓	✓
H ₂ O	✗	✓
CH ₃ COCH ₃	✓	✓
CH ₂ Cl ₂	✓	✗
HCON(CH ₃) ₂	✓	✓
CH ₃ CN	✓	✓
(CH ₂) ₄ O	✗	✓
CH ₃ OCH ₃	✗	✗
SO(CH ₃) ₂	✓	✓
CHCl ₃	✗	✗

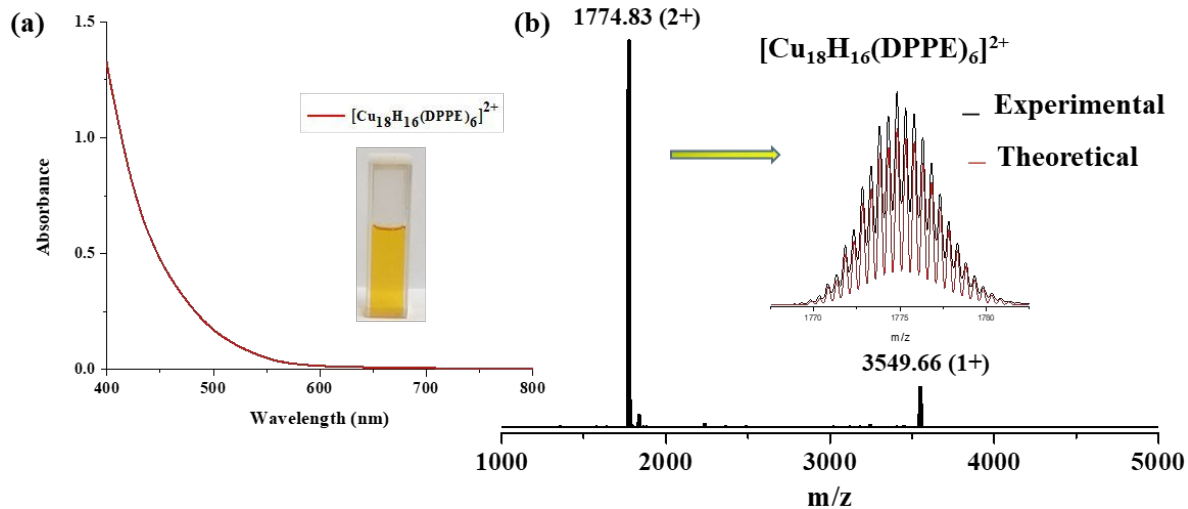


Figure S1. Characterization of $[\text{Cu}_{18}\text{H}_{16}(\text{DPPE})_6]^{2+}$ nanocluster. a) UV-vis spectrum (inset shows a photographic image of Cu_{18} NC in dichloromethane). b) ESI MS spectrum in the positive ion mode (inset shows good agreement between experimental and theoretical spectra).

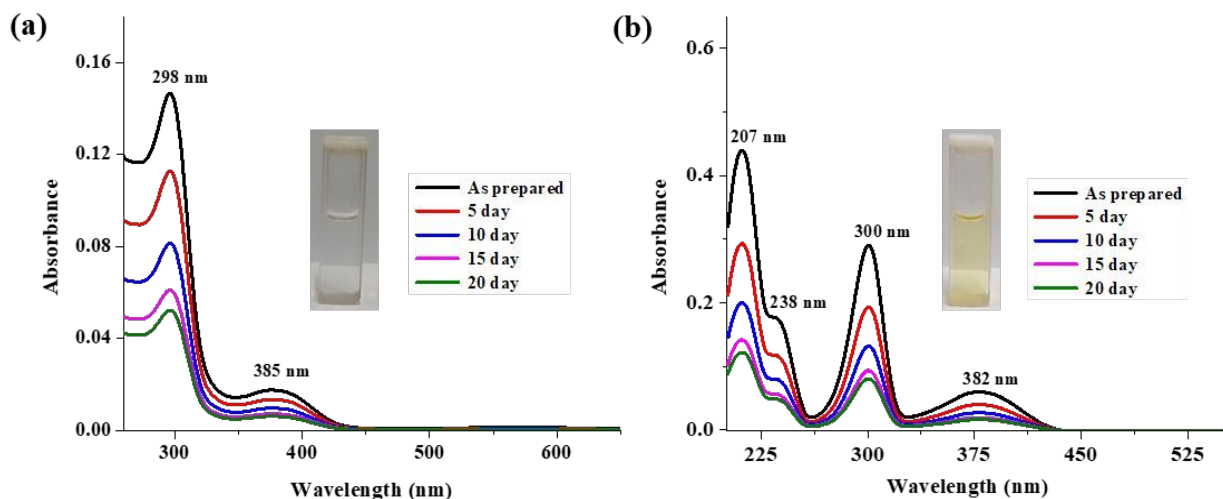


Figure S2. UV-vis. absorption spectra of (a) Cu_4 and (b) Cu_6 NCs in acetonitrile solvent. Insets show photographs of the solutions.

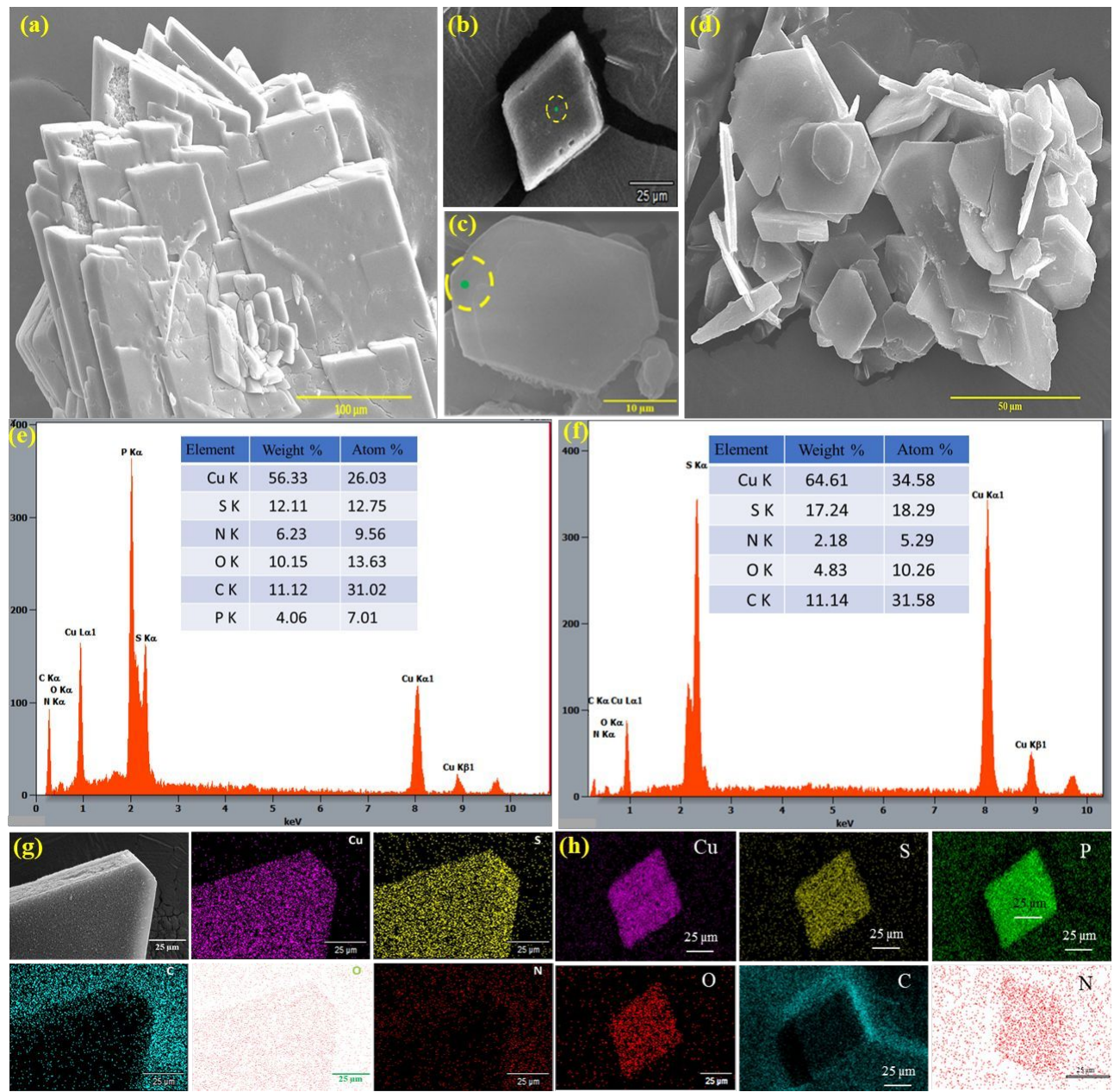


Figure S3. FESEM images of agglomerated single crystals of (a) Cu₄ and (d) Cu₆ NCs, (b, c) single crystals to determine EDS mapping, (e, f) EDS spectra of the same (inset shows weight and atomic percentages, respectively), (g, h) EDS mapping of each element present in Cu₄ and Cu₆ NCs.

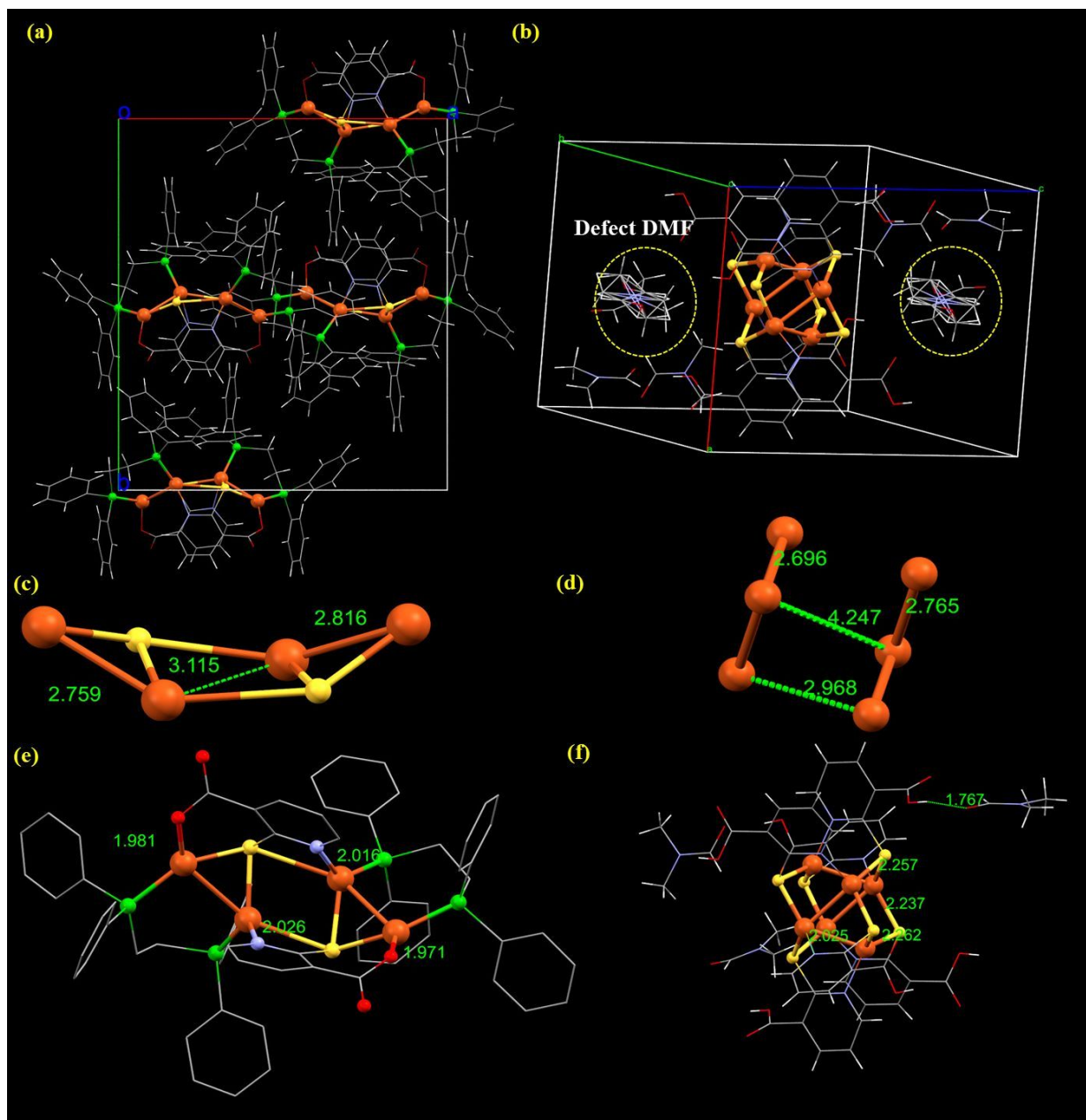


Figure S4. Structural packing per unit cell of (a) Cu_4 and (b) Cu_6 NCs. (c,e) Bond distances in Cu_4 and (d,f) Cu_6 NC along b-axis. Atomic color code: Orange=copper, yellow=S, Red=oxygen, blue=nitrogen, grey=carbon and white=hydrogen.

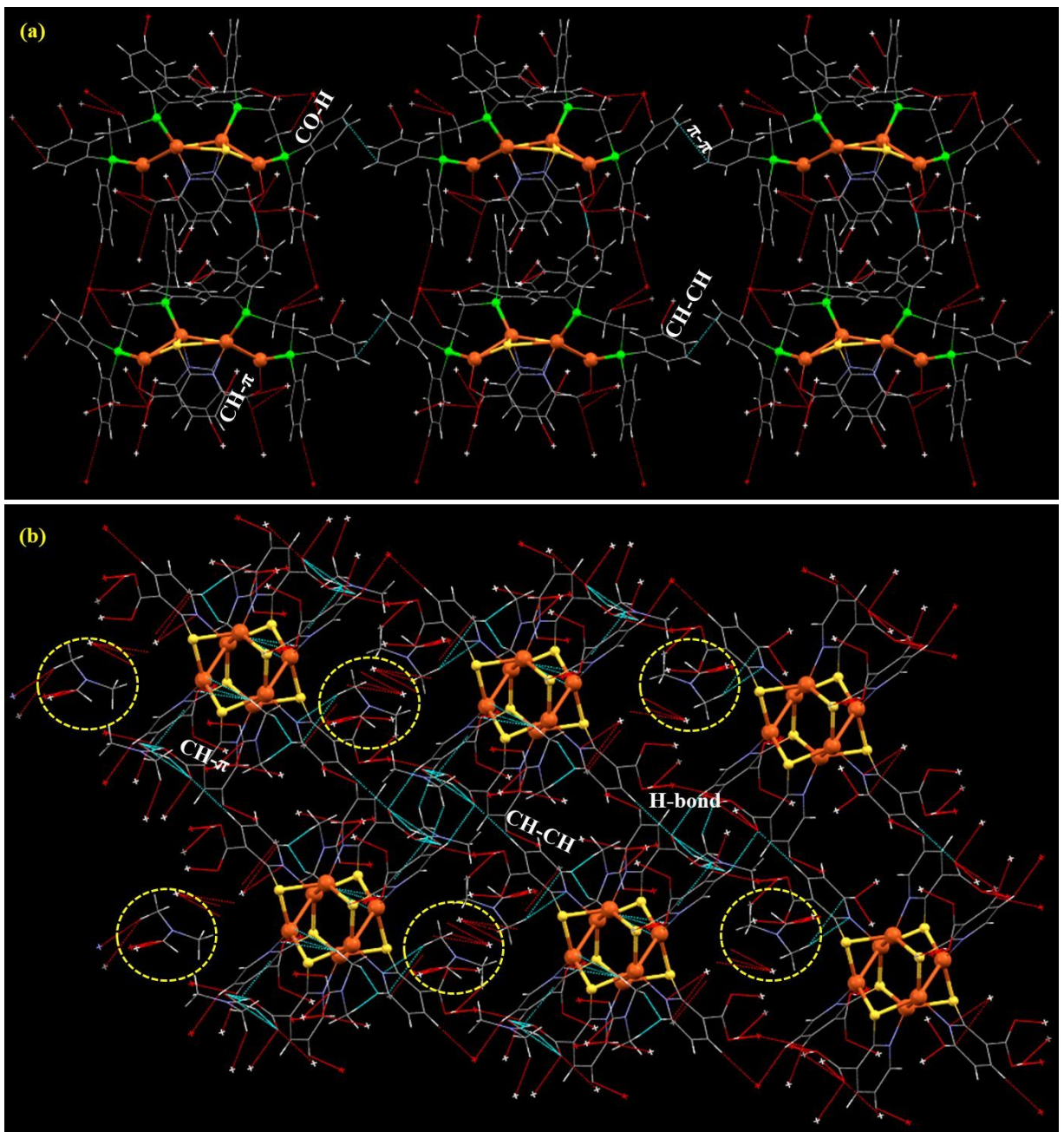


Figure S5. Ligand-centered non-covalent short contact interactions involve solid-state supramolecular packing of (a) Cu₄ and (b) Cu₆ NCs. Atomic color code: Orange=copper, yellow=S, Red=oxygen, blue=nitrogen, grey=carbon and white=hydrogen.

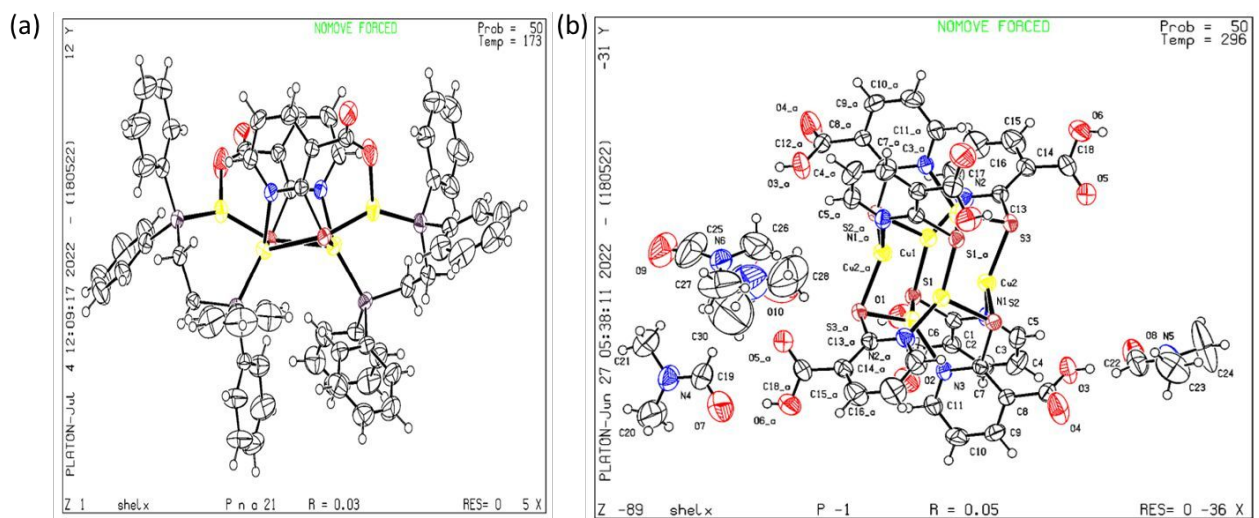


Figure S6. ORTEP structures of (a) Cu₄ and (b) Cu₆ NCs having 50% thermal ellipsoid parameters.

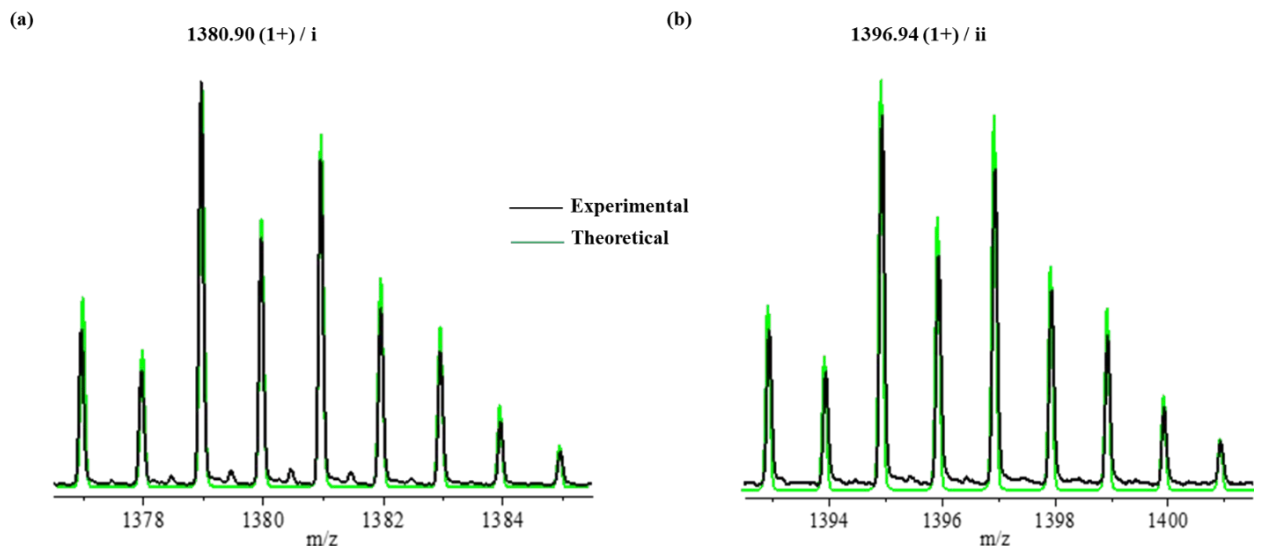


Figure S7. (a,b) Experimental and theoretical mass spectra of sodium and potassium attached to Cu₄ NC.

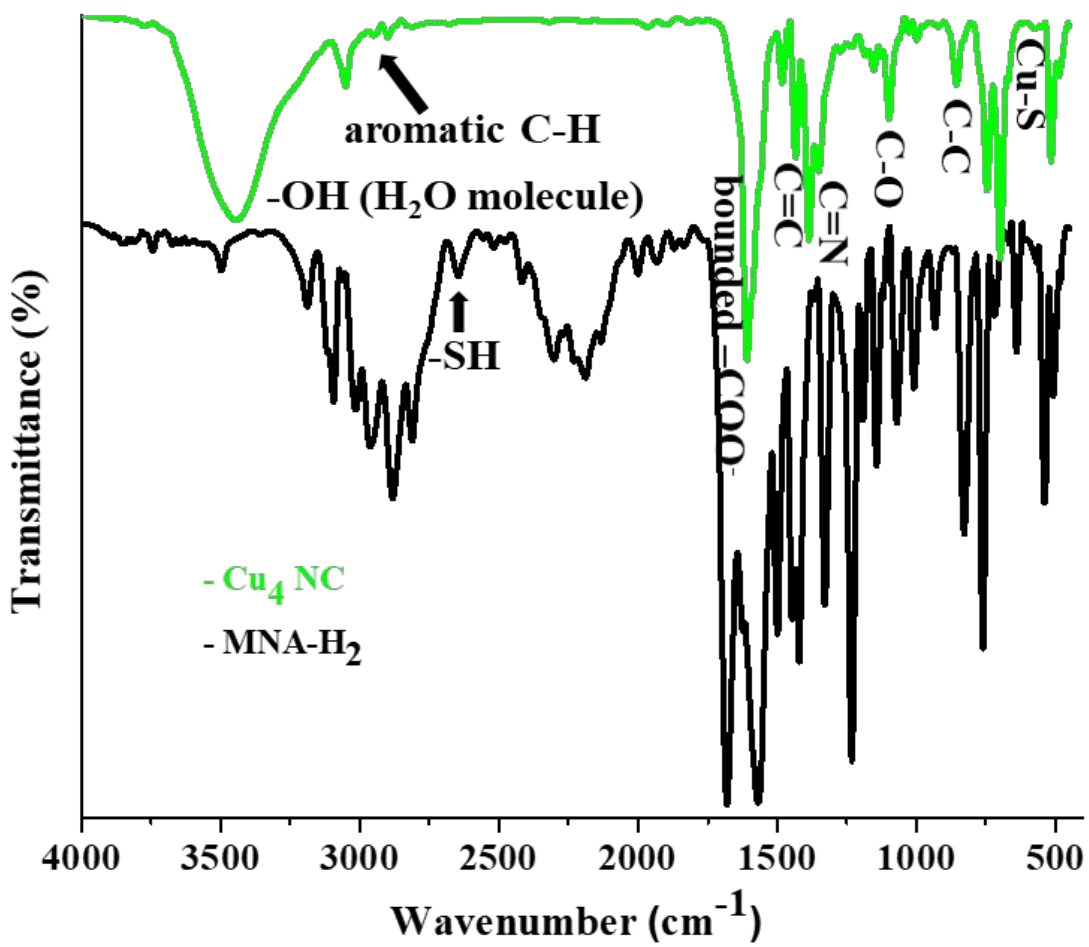


Figure S8. FTIR spectrum of $\text{Cu}_4 \text{ NC}$ compared with that of the free ligand. Stretching vibrations are mentioned.

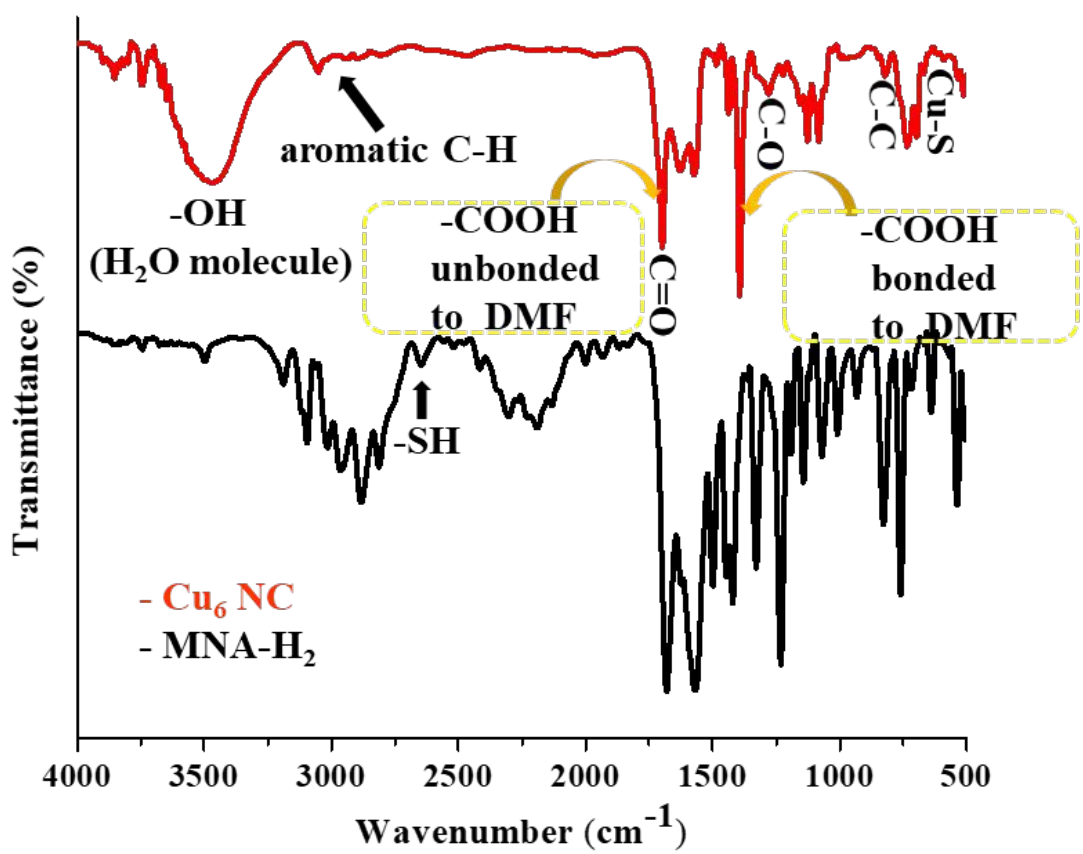


Figure S9. FTIR spectrum of $\text{Cu}_6 \text{ NC}$ compared with that of the free ligand. Stretching vibrations are mentioned.

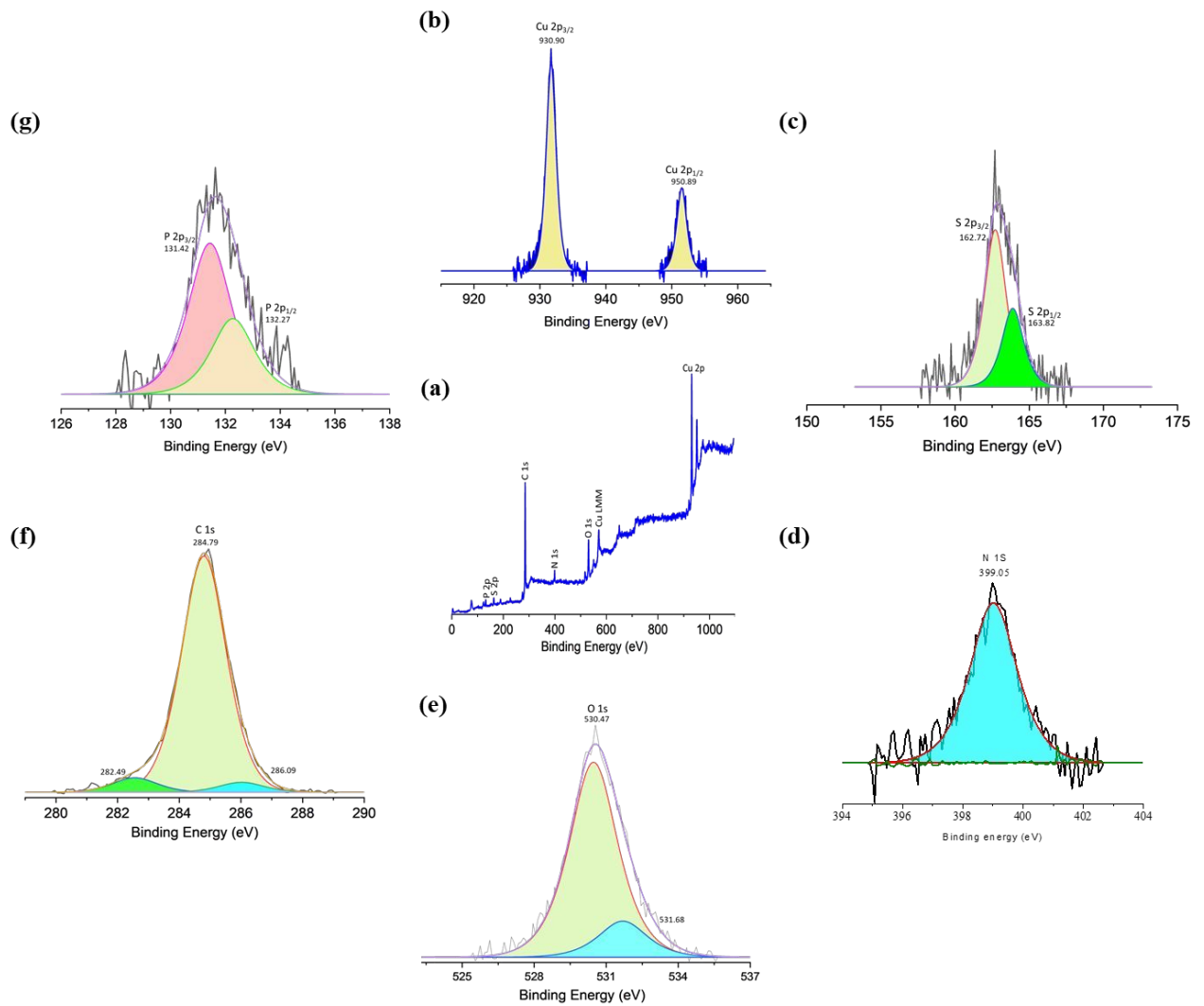


Figure S10. XPS spectrum of Cu₄ NC. (a) Survey spectrum of the respective elements. Expanded peak fittings of (b) Cu 2p, (c) S 2p, (d) N 1s, (e) O1s, (f) C 1s, and (g) P 2p spectral regions.

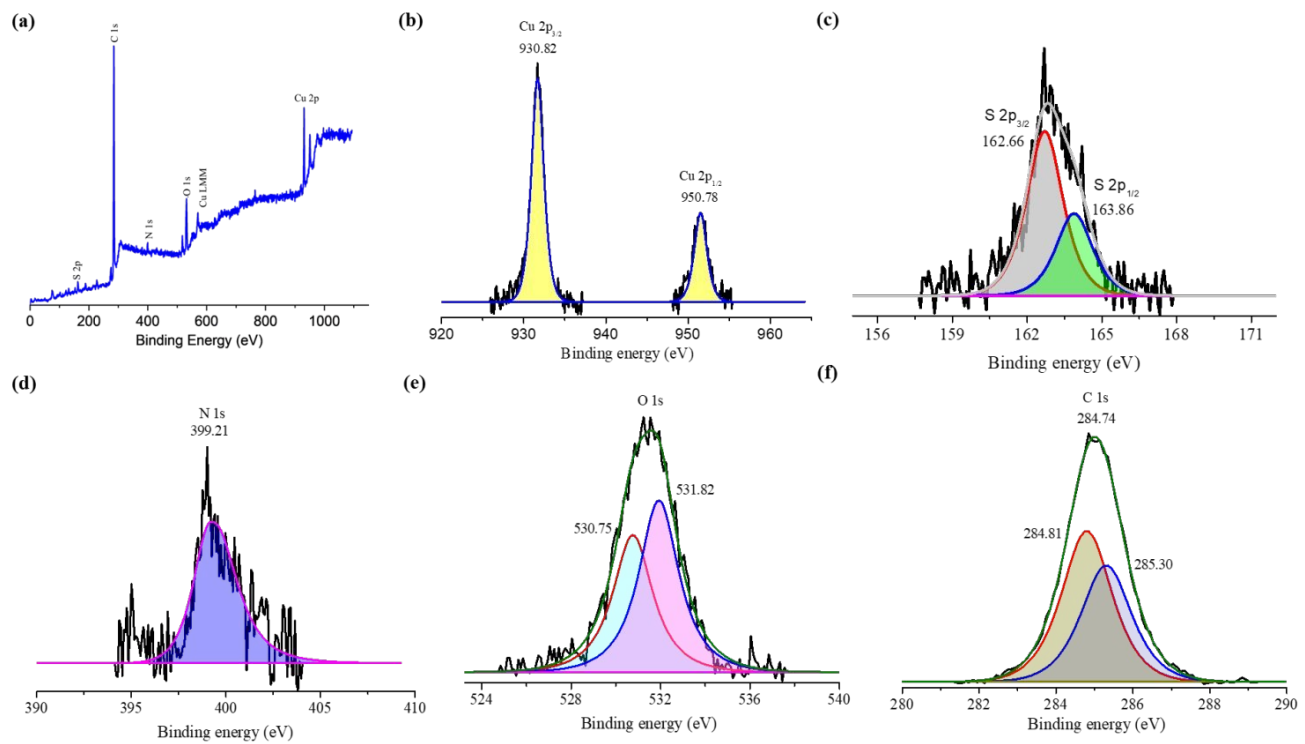


Figure S11. XPS spectrum of Cu₆ NC. (a) Survey spectrum of respective elements. Expanded peak fitting of (b) Cu 2p, (c) S 2p, (d) N 1s, (e) O 1s, (f) C 1s spectral regions.

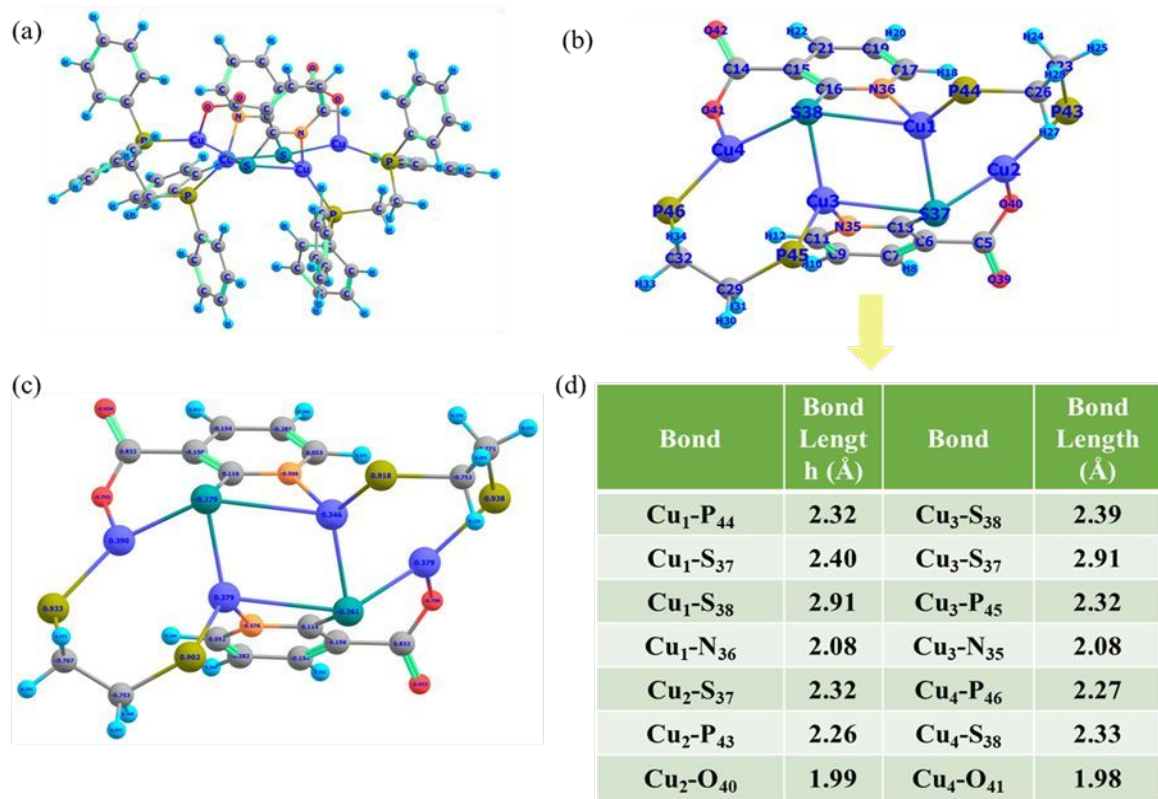


Figure S12. DFT optimized structural details of Cu_4 NC. (a) Full structure, (b) core cluster, (c) NBO charge distribution, and (d) bond distances in the optimized structure.

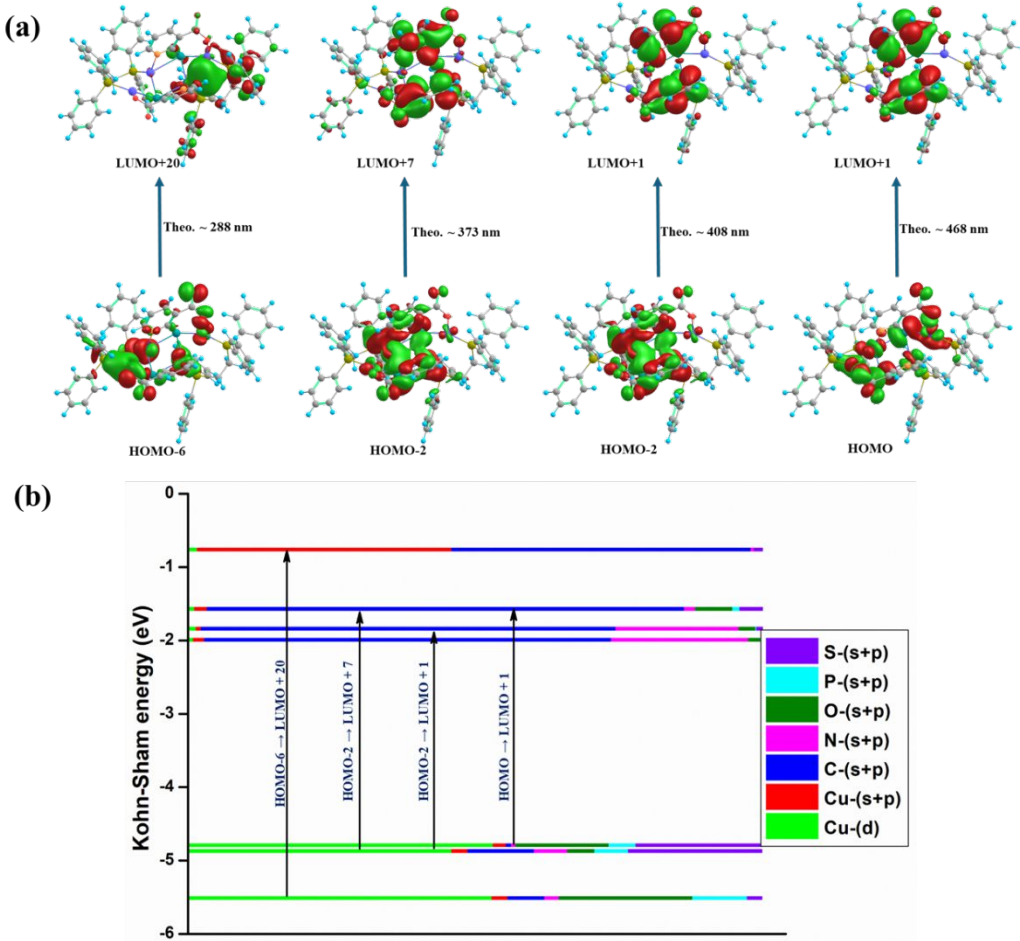


Figure S13. (a) Molecular orbitals involved in the electronic transitions of Cu_4 NC, calculated from TDDFT, (b) Khan-Sham molecular orbital diagram of Cu_4 NC.

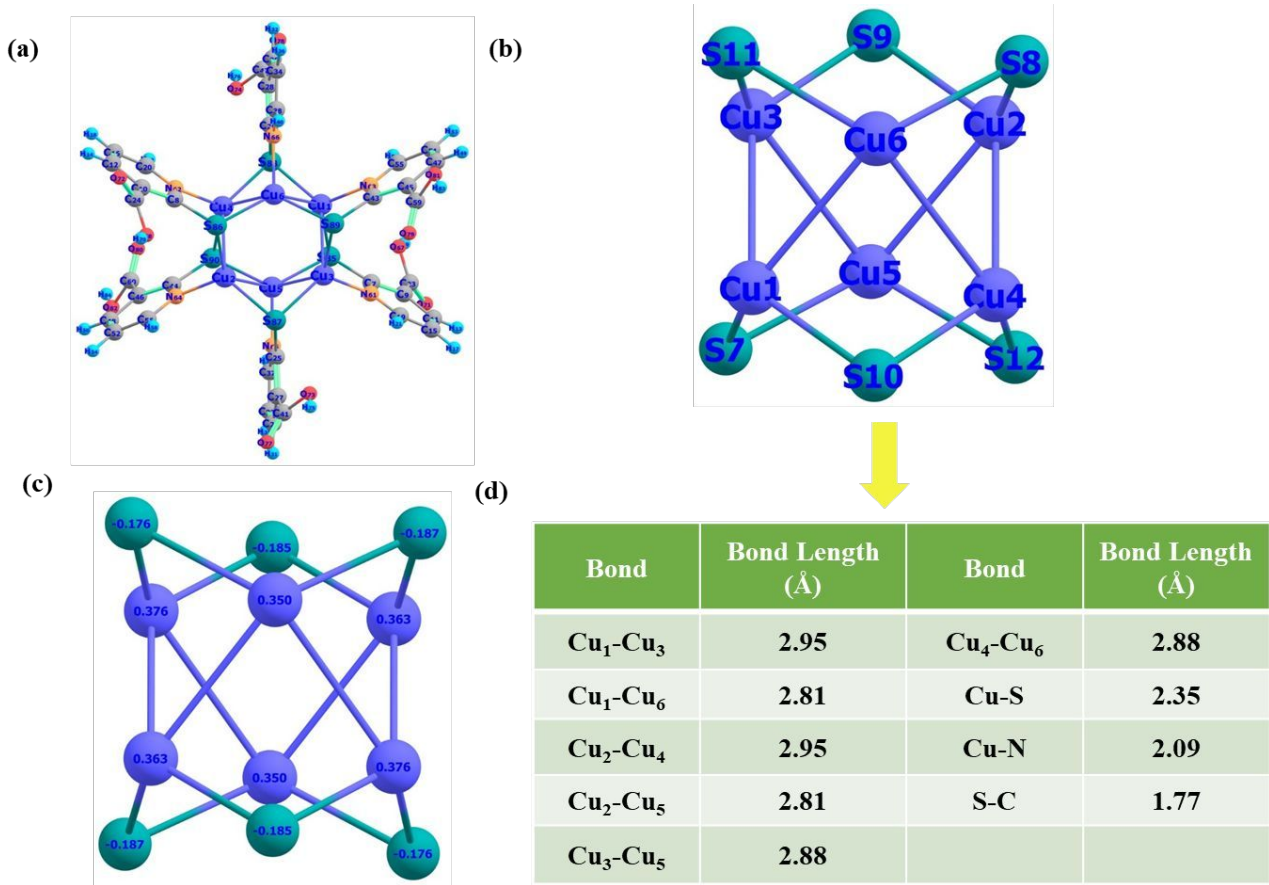


Figure S14. DFT optimized structural details of Cu_6 NC. (a) Full structure, (b) core cluster, (c) NBO charge distribution and (d) bond distances in the optimized structure.

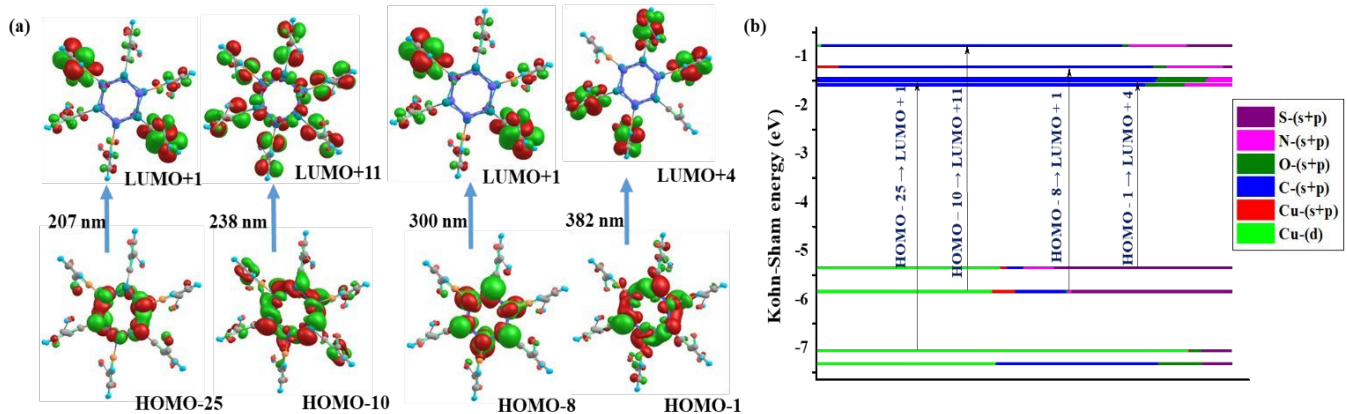


Figure S15. (a) Molecular orbitals involved in the electronic transition of Cu_6 NC, calculated from TDDFT, (b) Khan-Sham molecular orbital diagram of Cu_6 NC.

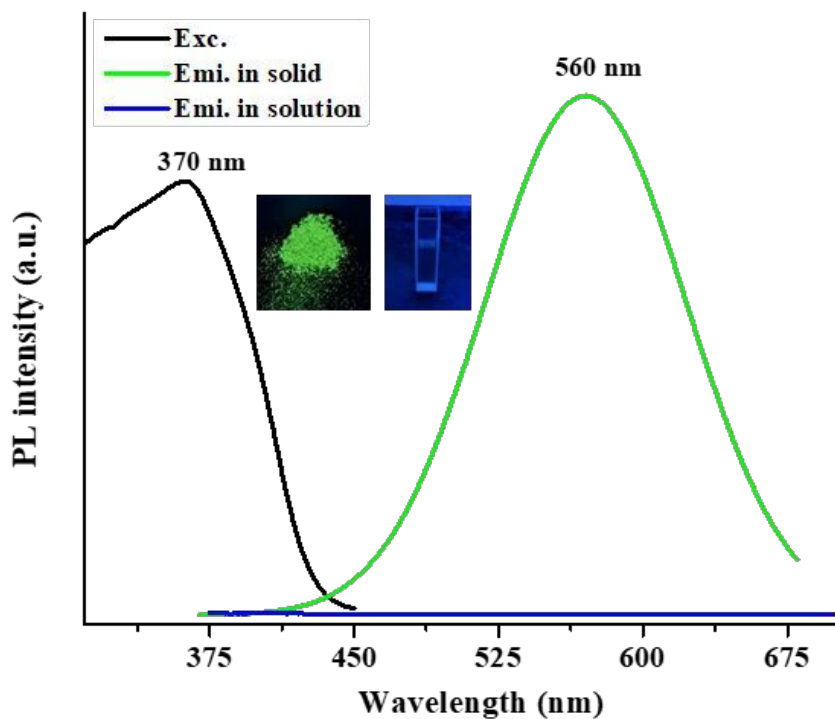


Figure S16. Photoluminescence emission spectrum of $\text{Cu}_4 \text{NC}$ in the solid and solution state. Inset shows the optical photographs of the cluster under UV light.

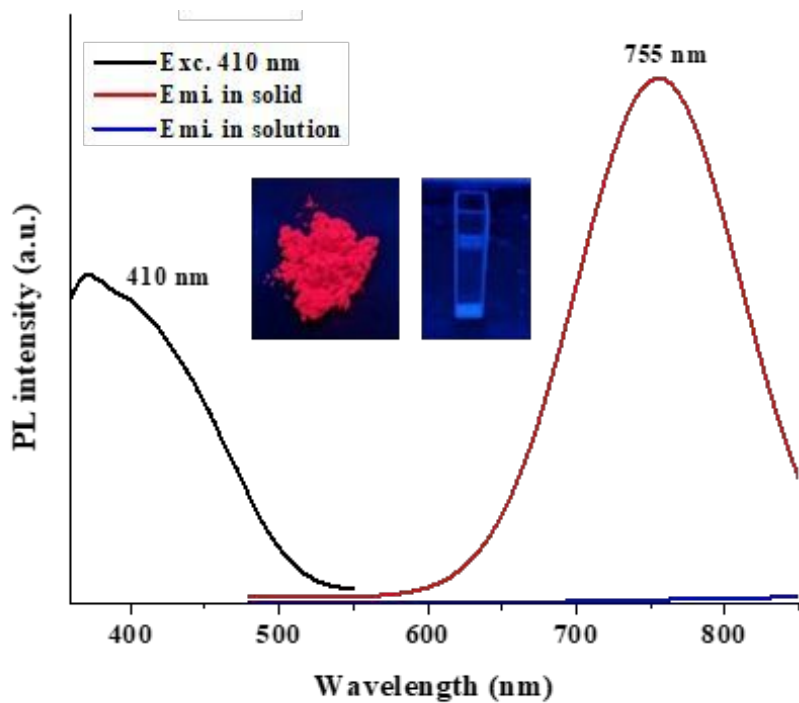


Figure S17. Photoluminescence emission spectrum of $\text{Cu}_6 \text{NC}$ in the solid and solution states. Inset shows the optical photographs of the cluster under UV light.

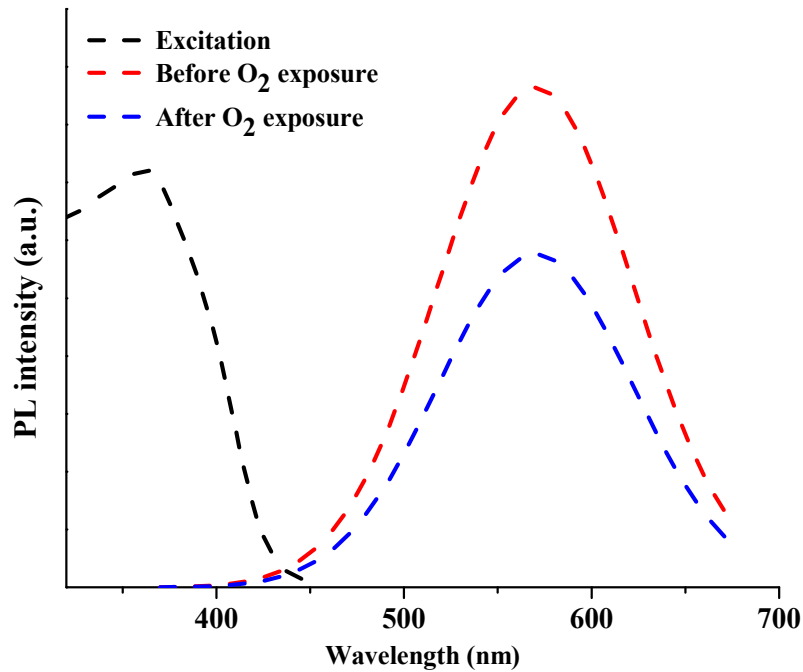


Figure S18. Photoluminescence (PL) emission spectra of Cu₄ NC in the solid state before and after O₂ exposure (Exc. 370nm and Emi. 560 nm).

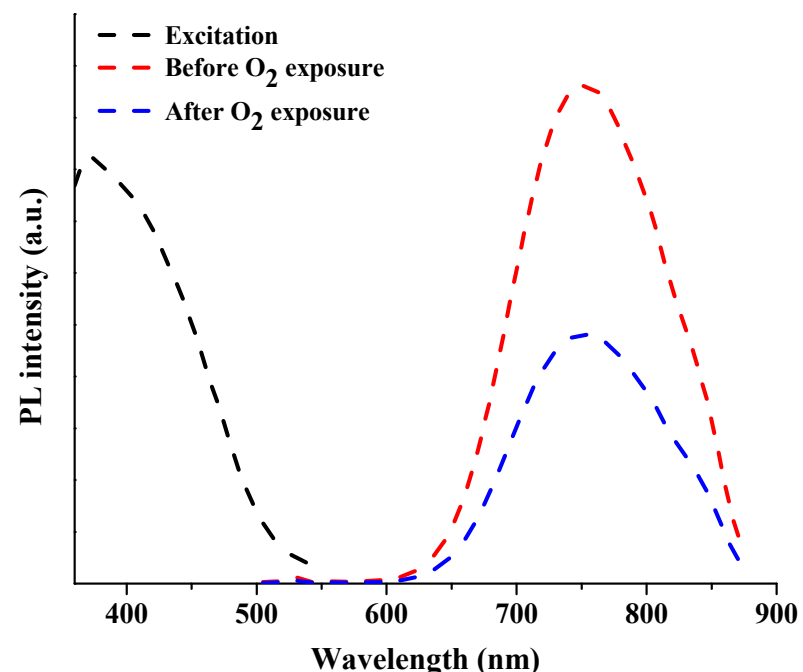


Figure S19. Photoluminescence (PL) emission spectra of Cu₆ NC in the solid state before and after O₂ exposure (Exc. 410 nm and Emi. 755 nm).

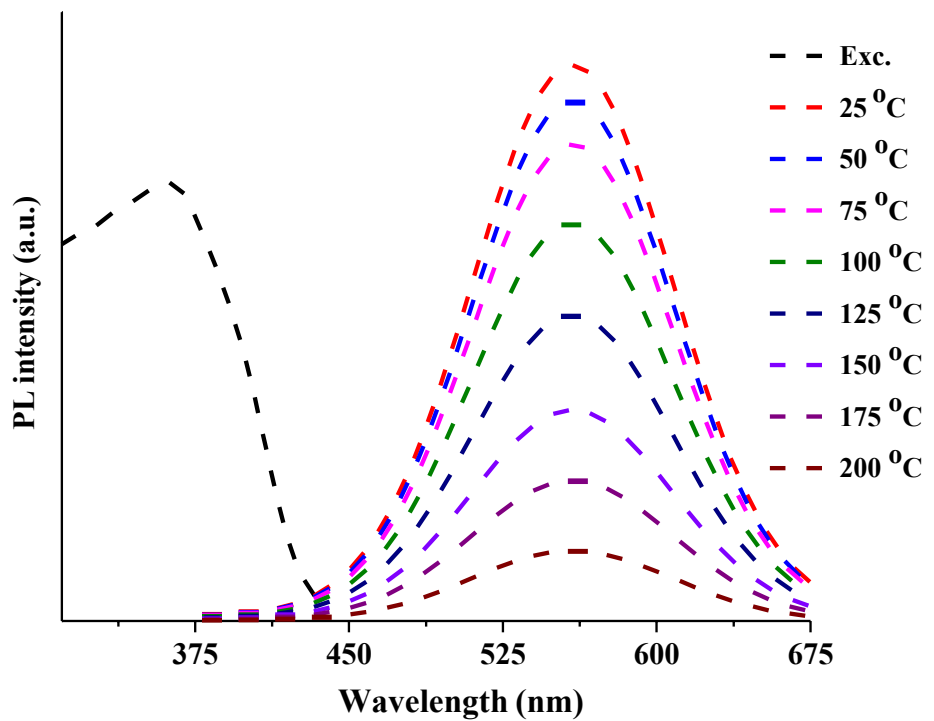


Figure S20. Photoluminescence emission spectra of Cu_4 NC crystals upon heating at different temperatures (Excitation at 370 nm and emission at 560 nm).

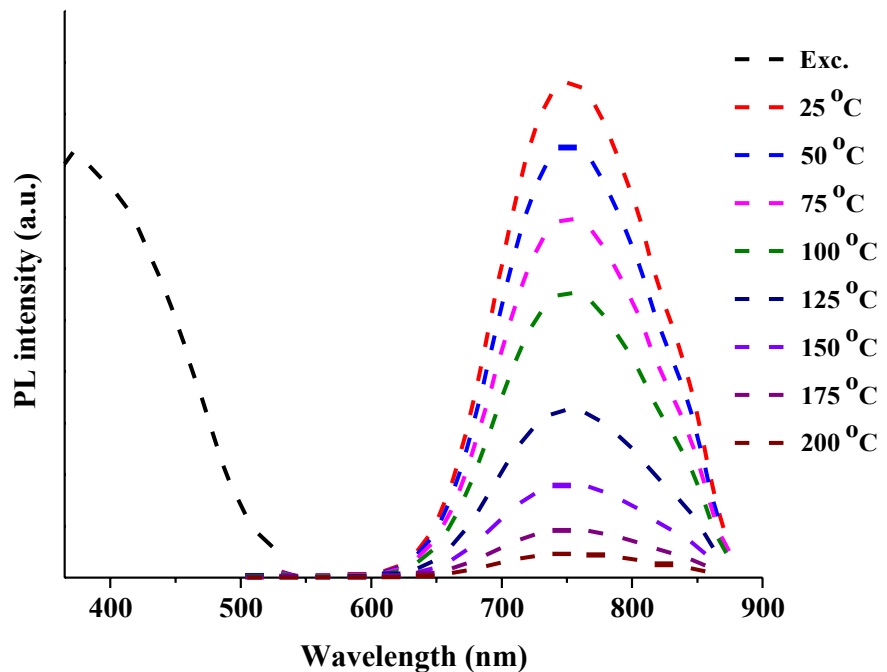


Figure S21. Photoluminescence emission spectra of Cu_6 NC crystals upon heating at different temperatures (Excitation at 410 nm and emission at 755 nm).

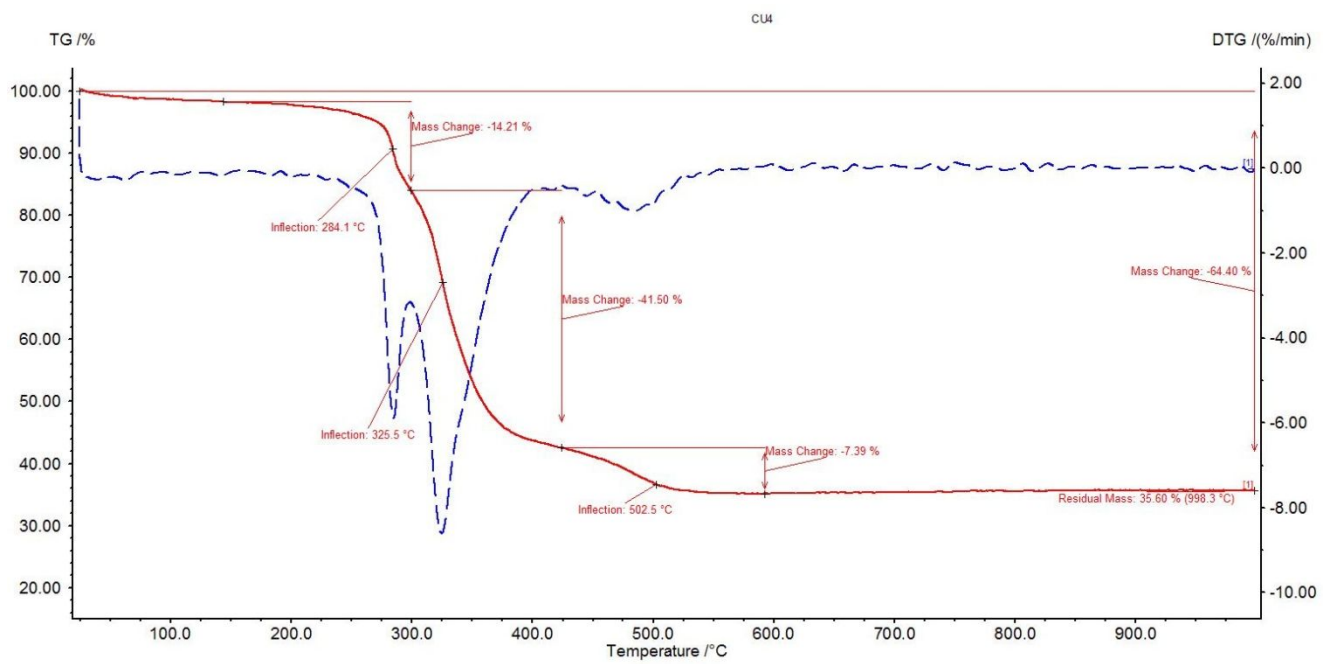


Figure S22. Thermogravimetry (TG) and derivative thermogravimetry (DTG) of Cu₄ NC. Initial mass loss is likely to be due to the fragmentation of ligands.

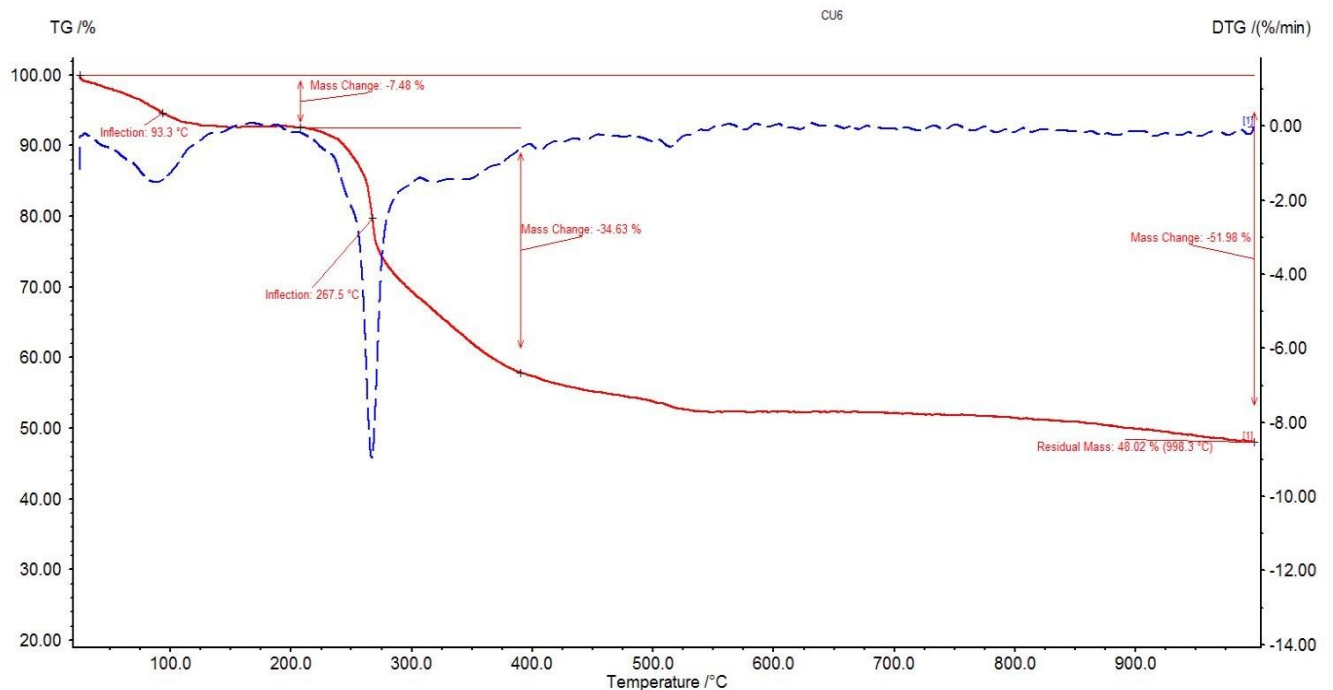


Figure S23. TG and DTG traces of Cu₆ NC. Initial mass loss is likely to be due to the solvent molecules.

2. References

- (1) Perruchas, S.; Le Goff, X.F.; Maron, S.; Maurin, I.; Guillen, F.; Garcia, A.; Gacoin, T.; Boilot, J.P. Mechanochromic and thermochromic luminescence of a copper iodide cluster. *J. Am. Chem. Soc.* **2010**, 132(32), 10967-10969.
- (2) Kitagawa, H.; Ozawa, Y.; Toriumi, K. Flexibility of cubane-like Cu₄I₄ framework: temperature dependence of molecular structure and luminescence thermochromism of [Cu₄I₄(PPh₃)₄] in two polymorphic crystalline states. *Chem. Commun.* **2010**, 46(34), 6302-6304.
- (3) Jana, A.; Jash, M.; Jash, Dar, W.A. ; Roy, J.; Chakraborty, P.; Paramasivam, G.; Lebedkin, S.; Kirakci, K.; Manna; Antharjanam, S.; Machacek, J. ; Kucerakova, M. ; Ghosh, S.; Lang, K.; Kappes, M.M.; Base, T.; Pradeep, T. Carborane-thiol protected copper nanoclusters: stimuli-responsive materials with tunable phosphorescence. *Chem. Sci.* **2023**, 14, 1613-1626.
- (4) Wu, X.M.; Wang, J.Y.; Huang, Y.Z.; Chen, Z.N. Scissor-like Au₄Cu₂ Cluster with Phosphorescent Mechanochromism and Thermochromism. *Molecules* **2023**, 28(7), 3247.
- (5) Frisch, M. J.; Trucks, G. W.; Schlegel, H. B.; Scuseria, G. E.; Robb, M. A.; Cheeseman, J. R.; Scalmani, G.; Barone, V.; Mennucci,B.; Petersson, G. A. et al. *Gaussian 09*, Revision B.01; Gaussian Inc.:Wallingford, CT, **2009**.
- (6) Becke, A.D. Density-functional thermochemistry. I. The effect of the exchange-only gradient correction. *J. Chem. Phys.* **1992**, 96(3), 2155-2160.
- (7) Becke, A.D. Density-functional thermochemistry. IV. A new dynamical correlation functional and implications for exact-exchange mixing. *J. Chem. Phys.* **1996**, 104(3), 1040-1046.
- (8) Lee, C.; Yang, W.; Parr, R.G. Development of the Colle-Salvetti correlation-energy formula into a functional of the electron density. *Phys. Rev. B* **1988**, 37(2), 785.
- (9) Clark, T.; Chandrasekhar, J.; Spitznagel, G.W.; Schleyer, P.V.R. Efficient diffuse function-augmented basis sets for anion calculations. III. The 3-21+G basis set for first-row elements, Li-F. *J. Comput. Chem.* **1983**, 4(3), 294-301.
- (10) Hariharan, P.C.; Pople, J.A. The influence of polarization functions on molecular orbital hydrogenation energies. *Theor. Chim. Acta* **1973**, 28, 213-222.

- (11) Hay, P.J.; Wadt, W.R. Ab initio effective core potentials for molecular calculations. Potentials for the transition metal atoms Sc to Hg. *J. Chem. Phys.* **1985**, 82(1), 270-283.
- (12) Grimme, S.; Antony, J.; Ehrlich, S.; Krieg, H. A consistent and accurate ab initio parametrization of density functional dispersion correction (DFT-D) for the 94 elements H-Pu. *J. Chem. Phys.* **2010**, 132(15).
- (13) Lu, T.; Chen, F. Multiwfn: A multifunctional wavefunction analyzer. *J. Comput. Chem.* **2012**, 33(5), 580-592.
- (14) Kresse, G.; Furthmüller, J. Efficiency of ab-initio total energy calculations for metals and semiconductors using a plane-wave basis set. *Comput. Mater. Sci.* **1996**, 6(1), 15-50.
- (15) Perdew, J.P.; Burke, K.; Ernzerhof, M. Generalized gradient approximation made simple. *Phys. Rev. Lett.* **1996**, 77(18), 3865.
- (16) Perdew, J.P.; JP Perdew, K. Burke; M. Ernzerhof. *Phys. Rev. Lett.* **1996**, 77, 3765.
- (17) Blöchl, P.E. Projector augmented-wave method. *Phys. Rev. B* **1994**, 50(24), 17953.
- (18) Kresse, G.; Joubert, D. From ultrasoft pseudopotentials to the projector augmented-wave method. *Phys. Rev. B* **1999**, 59(3), 1758.